REPORT SSD-TR-90-44

(2)

AD-A228 844

DTIC FILE COPY

Threshold Voltage and I–V Characteristics of AlGaAs/GaAs MODFETs

Prepared by

R. J. KRANTZ, W. L. BLOSS, and M. J. O'LOUGHLIN
Electronics Research Laboratory
Laboratory Operations
The Aerospace Corporation
El Segundo, CA 90245

30 September 1990

Prepared for

SPACE SYSTEMS DIVISION
AIR FORCE SYSTEMS COMMAND
Los Angeles Air Force Base
P.O. Box 92960
Los Angeles, CA 90009-2960

This report was submitted by The Aerospace Corporation, El Segundo, CA 90245, under Contract No. F04701-88-C-0089 with the Space Systems Division, P.O. Box 92960, Los Angeles, CA 90009-2960. It was reviewed and approved for The Aerospace Corporation by M. J. Daugherty, Director, Electronics Research Laboratory. Capt Modl was the project officer for the Mission-Oriented Investigation and Experimentation (MOIE) Program.

This report has been reviewed by the Public Affairs Office (PAS) and is releasable to the National Technical Information Service (NTIS). At NTIS, it will be available to the general public, including foreign nationals.

This technical report has been reviewed and is approved for publication. Publication of this report does not constitute Air Force approval of the report's findings or conclusions. It is published only for the exchange and stimulation of ideas.

Janet M. Modl

JANET M. MODL, Capt, USAF
MOIE Project Officer
STC/SWL

Jonathan M. Emmes

JONATHAN M. EMMES, Maj, USAF
MOIE Program Manager
AFSTC/WCO OL-AB

UNCLASSIFIED
SECURITY CLASSIFICATION OF THIS PAGE

REPORT DOCUMENTATION PAGE

1a. REPORT SECURITY CLASSIFICATION Unclassified	1b. RESTRICTIVE MARKINGS
2a. SECURITY CLASSIFICATION AUTHORITY	3. DISTRIBUTION/AVAILABILITY OF REPORT Approved for public release; distribution unlimited.
2b. DECLASSIFICATION/DOWNGRADING SCHEDULE	
4. PERFORMING ORGANIZATION REPORT NUMBER(S) TR-0090(5925-01)-3	5. MONITORING ORGANIZATION REPORT NUMBER(S) SSD-TR-90-44
6a. NAME OF PERFORMING ORGANIZATION The Aerospace Corporation Laboratory Operations; 6b. OFFICE SYMBOL (If applicable)	7a. NAME OF MONITORING ORGANIZATION Space Systems Division
6c. ADDRESS (City, State, and ZIP Code) El Segundo, CA 90245-4691	7b. ADDRESS (City, State, and ZIP Code) Los Angeles Air Force Base Los Angeles, CA 90009-2960
8a. NAME OF FUNDING/SPONSORING ORGANIZATION; 8b. OFFICE SYMBOL (If applicable)	9. PROCUREMENT INSTRUMENT IDENTIFICATION NUMBER F04701-88-C-0089
8c. ADDRESS (City, State, and ZIP Code)	10. SOURCE OF FUNDING NUMBERS: PROGRAM ELEMENT NO. / PROJECT NO. / TASK NO. / WORK UNIT ACCESSION NO.

11. TITLE (Include Security Classification)
Threshold Voltage and I-V Characteristics of AlGaAs/GaAs MODFETs

12. PERSONAL AUTHOR(S)
Krantz, Richard J.; Bloss, Walter L; and O'Loughlin, Michael J.

13a. TYPE OF REPORT	13b. TIME COVERED FROM ____ TO ____	14. DATE OF REPORT (Year, Month, Day) 30 September 1990	15. PAGE COUNT 19

16. SUPPLEMENTARY NOTATION

17. COSATI CODES			18. SUBJECT TERMS (Continue on reverse if necessary and identify by block number)
FIELD	GROUP	SUB-GROUP	I-V Characteristics
			MODFETs

19. ABSTRACT (Continue on reverse if necessary and identify by block number)

A strong inversion model, in the depletion layer approximation, of the I-V characteristics for MODFETs has been developed. The model describes MODFET I-V characteristics from subthreshold through saturation, over nine orders of magnitude in current. The saturation current is calculated and used to derive the experimental threshold voltage, which is determined by extrapolation of the saturation current (or square root of the current) vs gate voltage to zero current. It is shown that, for certain regions of acceptor doping, the experimentally determined threshold voltage can differ appreciably from the strong inversion definition. We show that this discrepancy is due to the effect of the depletion layer charge in the saturation region. Inclusion of the depletion layer charge in the analysis accounts for this difference and the difference between the saturation device capacitance per unit area and the AlGaAs layer capacitance per unit area.

20. DISTRIBUTION/AVAILABILITY OF ABSTRACT ☐ UNCLASSIFIED/UNLIMITED ☒ SAME AS RPT. ☐ DTIC USERS	21. ABSTRACT SECURITY CLASSIFICATION Unclassified
22a. NAME OF RESPONSIBLE INDIVIDUAL	22b. TELEPHONE (Include Area Code); 22c. OFFICE SYMBOL

CONTENTS

FIGURES

I. INTRODUCTION

The dependence of the threshold voltage and radiation response of n-channel AlGaAs/GaAs modulation doped field-effect transistors (MODFETs) on acceptor doping density has been analyzed previously (Refs. 1 and 2). These analyses have been extended to describe the dependence of MODFET I-V characteristics on acceptor doping density. A triangular-well, one-subband, depletion layer model has been developed that applies over the range of I-V characteristics from subthreshold to saturation, some nine orders of magnitude in drain-source current.

For typical unintentional acceptor doping densities of 10^{13} to 10^{15} cm^{-3}, characteristic in molecular beam epitaxy (MBE) grown structures, we show that the experimentally derived threshold voltage differs from the strong inversion model threshold voltage (Ref. 1) by 0.25 V at acceptor densities of 10^{13} cm^{-3}. At acceptor densities of 10^{15} cm^{-3}, the difference between the strong inversion model and the experimental extrapolation for the threshold voltage is about 0.12 V.

Inclusion of the acceptor doping density is shown to account for the discrepancy between the AlGaAs layer and the device capacitance per unit area described in the literature (Ref. 3).

II. MODEL

The band structure of a typical AlGaAs(n)/GaAs heterojunction with a Schottky barrier, ϕ_m, at the gate and a spacer layer at the interface under bias, V_g, is shown in Fig. 1.

Under the restrictions imposed by the assumptions cited in the caption of Fig. 1, Poisson's equation may be integrated across the structure to yield the applied gate voltage as a function of device geometry, doping densities, and channel charge, n_s:

$$V_g = V_o + f(n_s) \tag{1}$$

where V_o is the difference between the Schottky barrier height and the sum of the AlGaAs/GaAs band offset and potential drop across the doped AlGaAs layer resulting from the ionized donors. The function $f(n_s)$ may be written as

$$f(n_s) = (q/\varepsilon)(d + a)(N_a W + n_s) + C_o(N_a W + n_s)^{2/3} + (kT/q)\ln[\exp(n_s n_c) - 1] \tag{2}$$

where C_o is a function of the Planck constant, the carrier effective mass, the elemental charge, and the permittivity of AlGaAs and GaAs, all assumed to be equal. C_o is equal to $\sim 1.7 \times 10^{-9}$ V-cm$^{4/3}$. Similarly, the charge density n_c is a function of physical constants and the effective mass of the carriers and is equal to $\sim 8.4 \times 10^{11}$ cm^{-2}. In the next section, we will exploit the mathematical properties of the function $f(n_s)$ to derive the electrical properties of these devices.

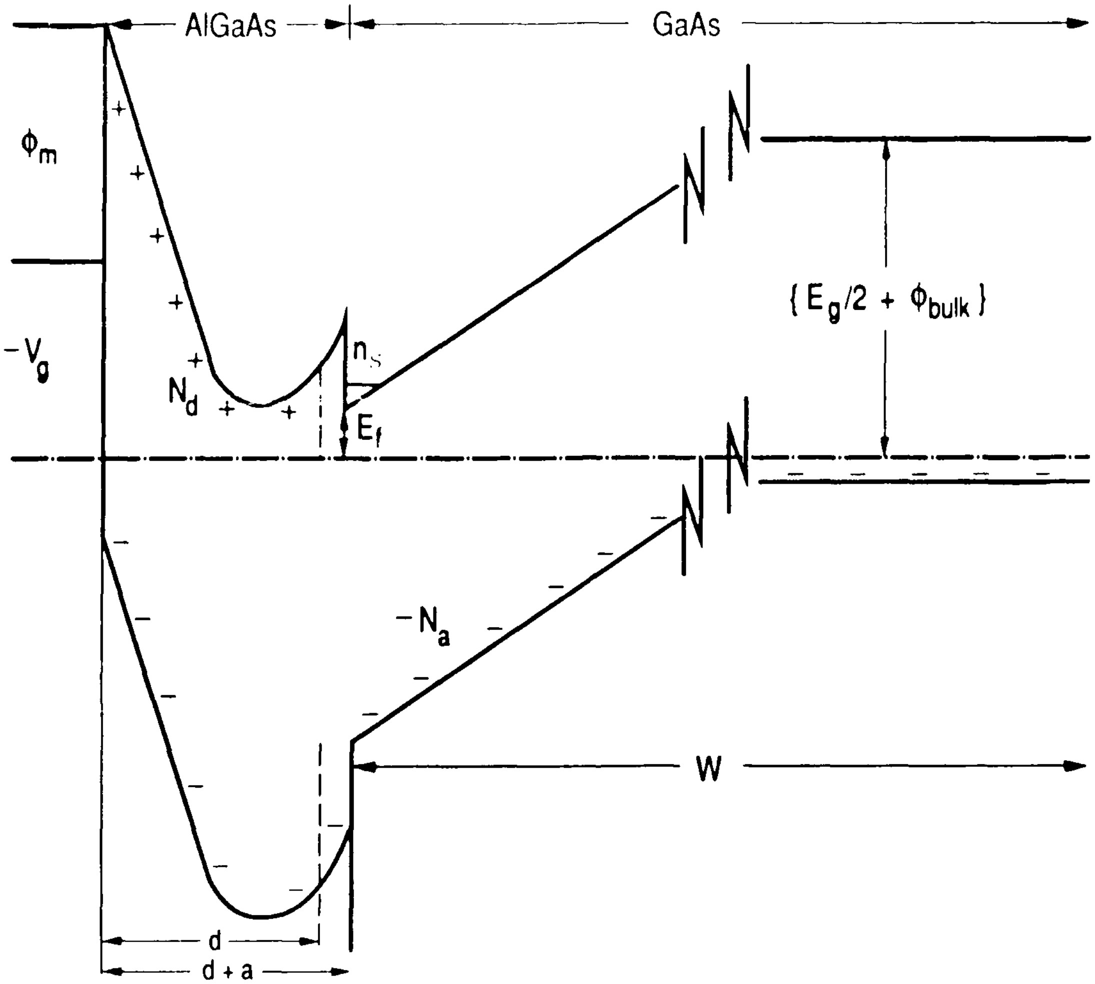

Fig. 1. Band Diagram of a Typical AlGaAs(n)/GaAs MODFET with Schottky Gate, Under Bias. In the depletion layer approximation, the donors and acceptors are assumed to be completely ionized in the doped AlGaAs layer, d, the spacer layer, a, and the depletion layer, W. The doping densities, N_d and N_a, are assumed to be constant. A delta-function channel charge distribution at the average channel width is assumed. Band bending from the interface at (d + a) to the edge of the depletion region (W + d + a) is the difference of position of conduction band relative to the Fermi level, $E_g/2 + \phi_{bulk}$, and the Fermi level relative to the bottom of the two-dimensional channel, E_f.

III. ELECTRICAL PROPERTIES

A. THRESHOLD VOLTAGE

At threshold, we require that the channel density be equal to the acceptor density, N_a, times the average channel width, z_{av}, which may be calculated in the triangular-well approximation using variational wave functions (Ref. 4). This definition for threshold is consistent with the strong inversion definition of threshold in metal oxide semiconductor field effect transistors (MOSFETs). Our definition is the two-dimensional equivalent. Evaluating Eq. (2) at threshold and substituting into Eq. (1) yields the threshold voltage. The results of this calculation indicate that the threshold voltage is very sensitive to the acceptor doping density above $\sim 10^{14}\ cm^{-3}$. The details of this calculation have been presented elsewhere (Ref. 1).

B. SUBTHRESHOLD I-V CHARACTERISTICS

In the subthreshold region, where $n_s < N_a z_{av}$ over the whole channel, $f(n_s)$ may be approximated as follows:

$$f(n_s) = (kT/q)\ln[g(n_s)] \tag{3}$$

Solving Eq. (3) for $g(n_s)$, expanding to first order about the threshold charge, and using Eq. (2) to determine the Taylor series expansion coefficients yield a convenient approximation for $f(n_s)$ when substituted back into Eq. (3). Shown in Fig. 2 is the function $f(n_s)$, which is equivalent to $(V_g - V_o)$ vs the log of the channel charge for two values of the acceptor doping density. The long dashes are the results of the approximation just described.

Using the subthreshold approximation for $f(n_s)$ in Eq. (1), and solving for n_s in terms of V_g, we may calculate the subthreshold I-V characteristics using a charge control model (Ref. 5). The results of this calculation yield the MODFET equivalent of the MOSFET charge sheet subthreshold characteristics (Ref. 6). Details of these results will be discussed at the end of this

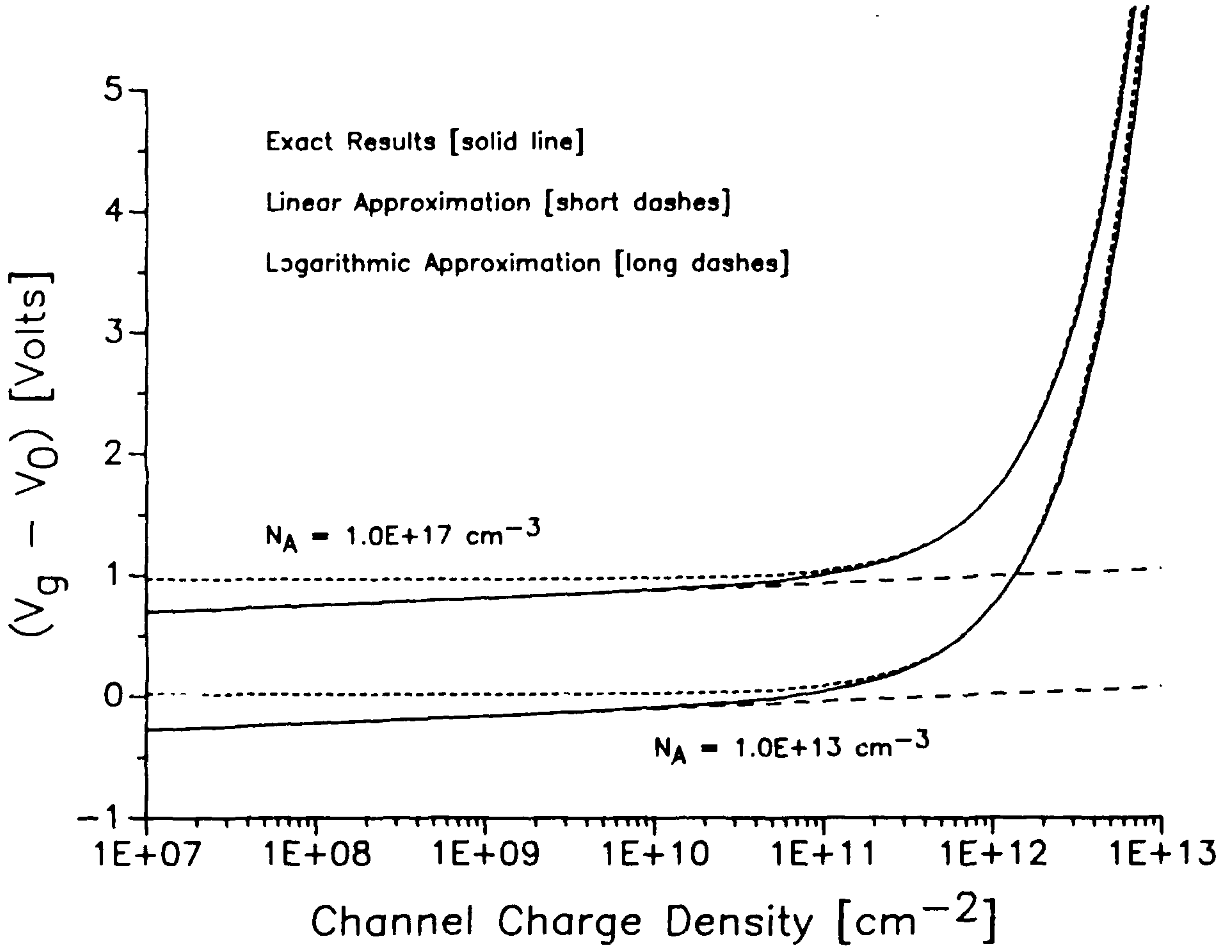

Fig. 2. $V_g - V_0$ vs the Log of the Channel Charge. The solid lines are the results given by Eq. (2). The long dashes are the results of the Taylor expansion of $f(n_s)$ in subthreshold, as described in the text. For an acceptor doping density of 10^{13} cm^{-3}, the threshold charge density is less than 10^8 cm^{-2}. Therefore, the subthreshold expansion is useful well above the threshold charge density. At an acceptor doping density of 10^{17} cm^{-3}, the threshold density is near 10^{11} cm^{-2}, and this expansion is only useful for channel charge densities below threshold. The short dashes are the results of a Taylor expansion of $f(n_s)$ about n_c, as described in the text.

section in the context of the complete description of I-V characteristics from subthreshold to saturation.

C. SATURATION I-V CHARACTERISTICS

We define the saturation region such that $n_s > n_c$ over the whole channel. In this region, Eq. (2) may be expanded in a Taylor series in n_s about n_c. The results of this approximation to first order are shown as short dashes in Fig. 2. Above n_c (8.4×10^{11} cm^{-2}), the expansion is quite good. Much below n_c (3×10^{11} cm^{-2}), the first order expansion departs from the exact result and approaches a constant at low channel densities for all acceptor densities. As before, the approximation for $f(n_s)$ may be substituted into Eq. (1), which is inverted to yield n_s as a function of V_g. The result is

$$n_s = n_c + K^{-1}[V_g - V_o - f(n_c)]/(kT/q) \qquad (4)$$

where K is a constant that depends on the device geometry, doping densities, depletion width, and physical constants. This form for n_s is different than the form previously assumed (Ref. 5). The previous form ignores the contribution from n_c and $f(n_c)$ and implicitly assumes that K^{-1} is $(kT/q)C_{A\ell GaAs}$. The charge control model may then be used to calculate saturation I-V characteristics. We will defer the detailed discussion of these results to the end of this section.

D. DEVICE CAPACITANCE

The device capacitance, when the charge density in the channel is greater than n_c, may be determined by differentiating Eq. (4) with respect to V_g. The resulting capacitance per unit area, C_{area}, may be cast in the following form (Ref. 3):

$$C_{area} = \varepsilon/(d + a + \Delta d) \qquad (5)$$

where Δd is given by

$$\Delta d = (2\varepsilon/3q)C_o(N_aW + n_c)^{1/3} + 1.58(kT\varepsilon/q^2)/n_c \qquad (6)$$

When $N_a W \ll n_c$, Δd is ~ 90 Å. For large values of the acceptor doping density (~ 10^{17} cm^{-3}), Δd is reduced to ~ 75 Å. The constant K, in the previous subsection, is related to the capacitance per unit area as follows:

$$K^{-1} = (kT/q)C_{area} \tag{7}$$

E. EXPERIMENTAL THRESHOLD VOLTAGE

MODFET threshold voltages are determined experimentally by extrapolating the saturation current, or square root of the saturation current, vs gate voltage to zero. The gate voltage intercept is the experimentally determined threshold voltage. This is mathematically equivalent to solving Eq. (4) for the gate voltage when n_s is equal to zero. This calculation yields an experimental threshold voltage that differs from the strong inversion definition of the threshold voltage. The difference between the experimental value and the theoretical value is given by

$$\Delta V_{th} = f(n_c) - f(n_{th}) - qn_c/C_{area} \tag{8}$$

where $f(n_{th})$ is the value of Eq. (2) when evaluated at the threshold charge density. In Fig. 3, the threshold voltage difference is plotted vs the log of the acceptor density.

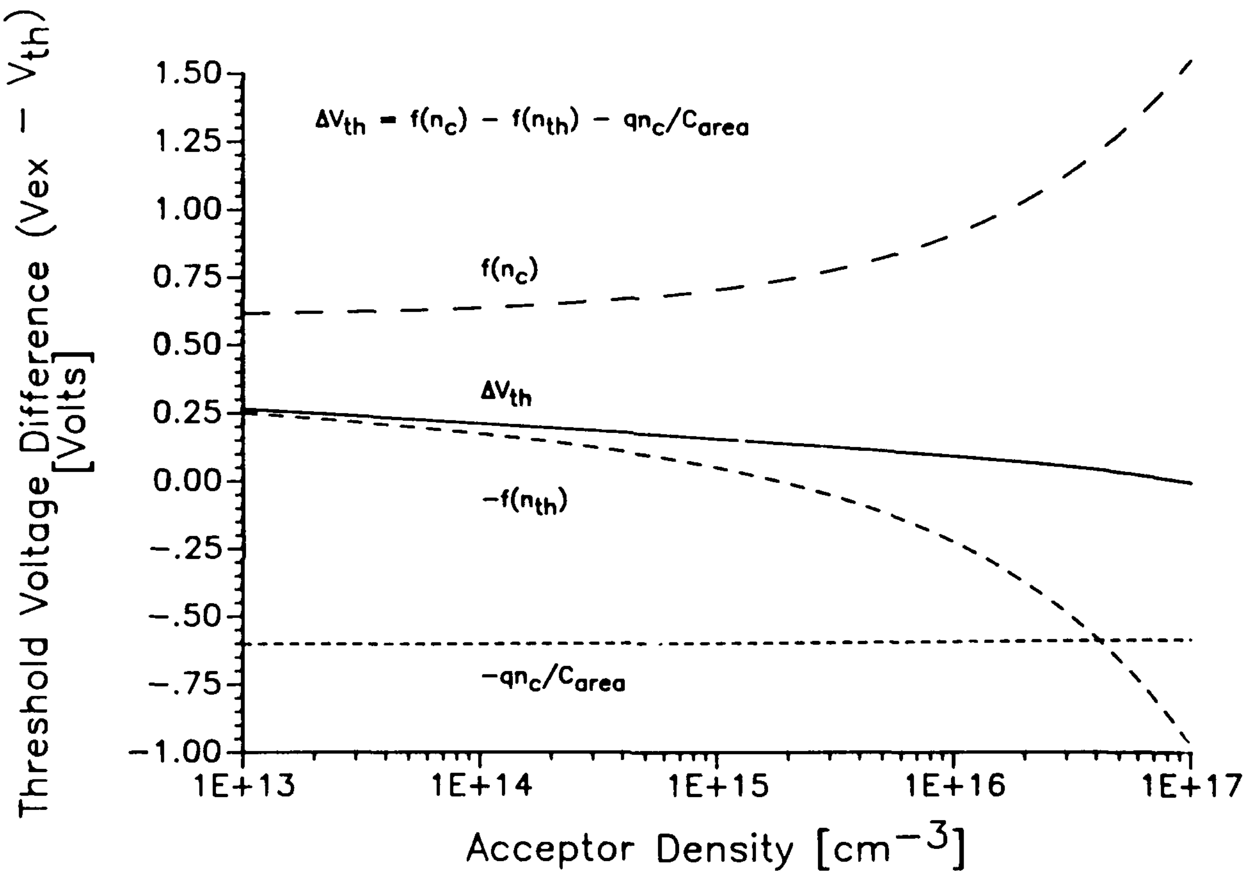

Fig. 3. Difference of the Experimental and the Strong Inversion Threshold Voltage vs the Log of the Acceptor Density. Each term in Eq. (8) is plotted separately. At low acceptor densities (< 10^{14} cm^{-2}), the difference may be as much as 0.25 V. This difference decreases as the acceptor density increases. Because this difference depends on the acceptor density, a comparison of experimental threshold voltages may not be appropriate if acceptor densities differ significantly.

IV. I-V CHARACTERISTICS FROM SUBTHRESHOLD TO SATURATION

In the charge control model, I-V characteristics are determined by substituting $V_g - V_c(x)$ for V_g in Eq. (1), inverting the result to find n_s as a function of $V_c(x)$, substituting the result into the relationship for the current at position x in the channel, and integrating over the channel length (Ref. 5). In the subthreshold and saturation regions, as defined in subsections III.B and III.C, the approximations for $f(n_s)$ permit a straightforward inversion of Eq. (1) for this purpose. As seen in Fig. 2, there is a region over which neither the subthreshold nor the saturation expansion applies. Because the integration for the current is performed over the voltage in the channel as well as over the channel length, an approximation must be determined that is continuous in the voltage, may be inverted to explicitly determine the channel charge in terms of the channel voltage, and reasonably approximates $f(n_s)$ over the region.

To satisfy these requirements, we have derived a piecewise approximation for $f(n_s)$ over this region. From the threshold charge to the channel charge, n_o, at which the exact $f(n_s)$ is halfway between the subthreshold approximation at threshold and the saturation approximation at n_c, we have approximated $f(n_s)$ as the log of a linear function of n_s. The two expansion coefficients are chosen so that this approximation for $f(n_s)$ is exact at n_o and connects with the subthreshold approximation at the threshold channel density. From n_o to n_c, we have assumed that $f(n_s)$ is linear in n_s. The two expansion coefficients are determined so that the approximation in this region is exact at the extremes, n_o and n_c.

The charge control model may now be used to calculate the I-V characteristics. A complication arises in the application of the charge control model because, for various values of the applied gate and drain-source voltages, different regions of the channel may have charge densities that must be calculated by different approximations to $f(n_s)$. Therefore, the current equation must be integrated placewise, although never over more than four regions, as

our piecewise approximation for $f(n_s)$ requires. Over a range of gate (or drain-source) voltages, 10 possible combinations of regions might occur. Shown in Fig. 4 is the drain-source current vs drain-source voltage, for the parameters given, for various gate voltages using the approximations just described.

In Fig. 5, we show the drain-source current vs applied gate voltage for three values of the acceptor density nd two values of the drain-source voltage.

Intrinsic transconductances may be calculated by differentiating the drain-source current relationships with respect to the gate voltage. Having done this calculation, we obtain transconductances of ~ 300 mS/mm for structures with acceptor doping of 10^{15} cm^{-3}, evaluated at zero gate voltage and 2.5 V drain-source voltage.

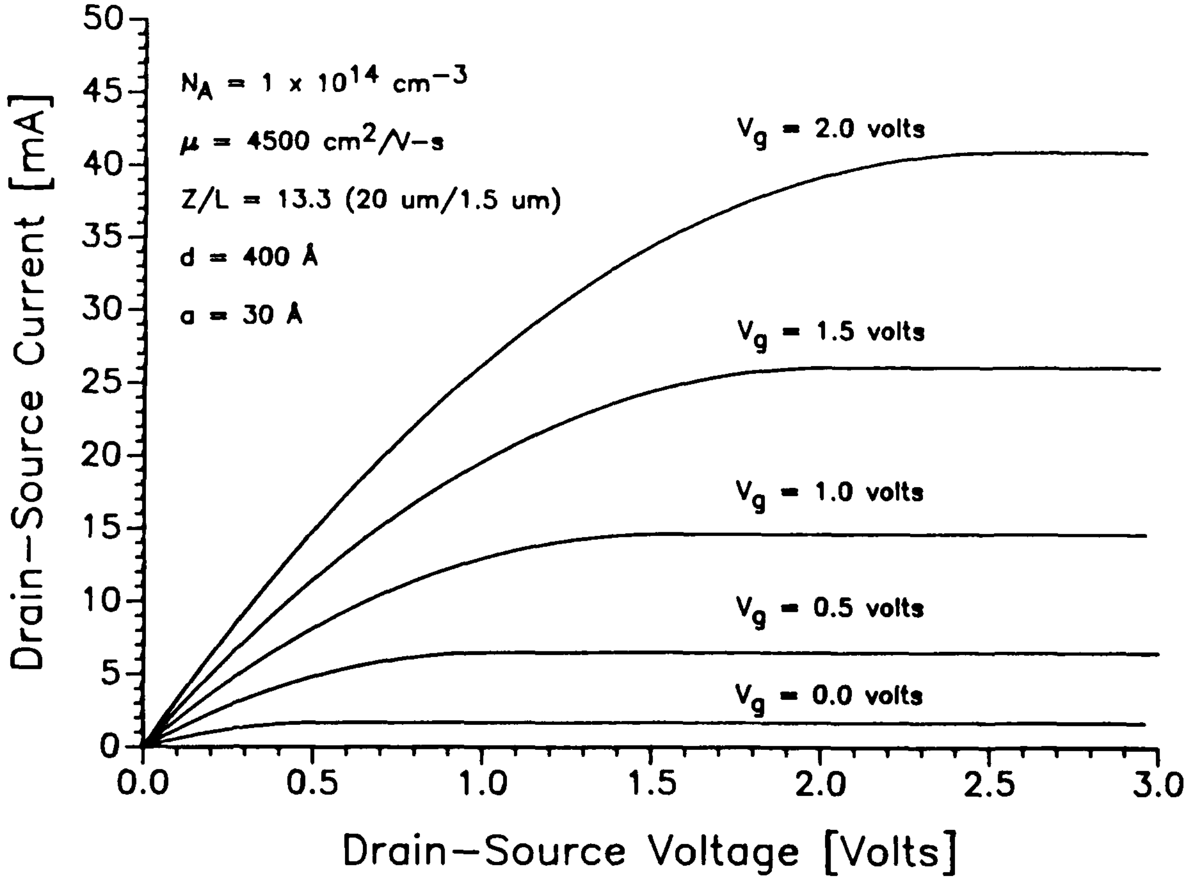

Fig. 4. Drain-Source Current vs Drain-Source Voltage. The current saturates at large drain-source voltage without velocity saturation or cutoff of the model invoked. When the whole channel is forced into the subthreshold charge region, the current depends on a constant plus an exponential in $-V_{ds}$ which is negligible at large drain-source voltages.

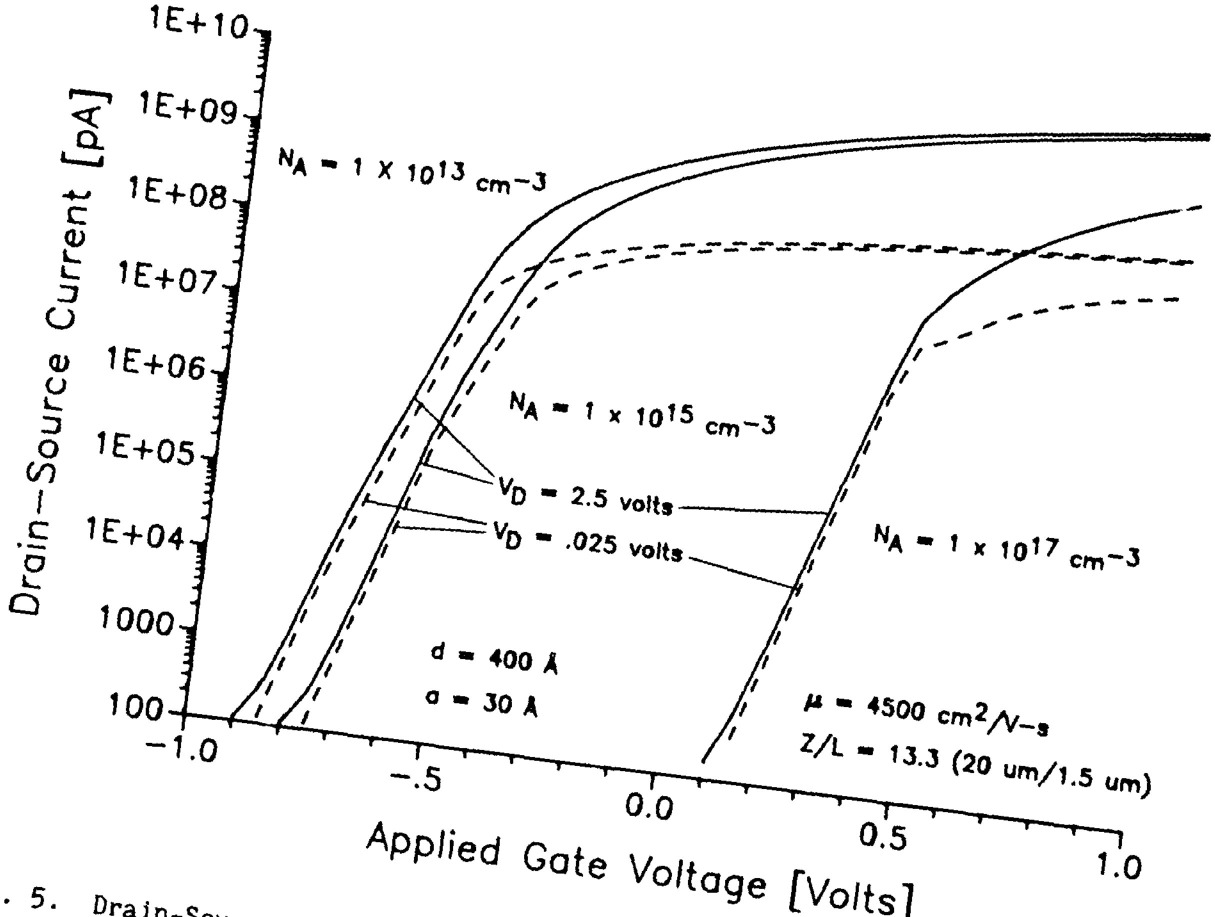

Fig. 5. Drain-Source Current vs Applied Gate Voltage. Current varies smoothly over nine orders of magnitude for all parameters except the highest acceptor density and smallest drain-source voltage. At high acceptor densities and low drain-source voltages, the approximations for $f(n_s)$ at the threshold charge density have significantly different slopes, resulting in a kink in the dashed curve at 0.5 V.

REFERENCES

1. R. J. Krantz and W. L. Bloss, "The Role of Unintentional Acceptor Concentration on the Threshold Voltage of Modulation-Doped Field-Effect Transistors," IEEE Trans. Electron Devices 36, 451-453 (1989).

2. R. J. Krantz, W. L. Bloss, and M. J. O'Loughlin, "High Energy Neutron Effects in GaAs Modulation-Doped Field Effect Transistors (MODFETs): Threshold Voltage," IEEE Trans. Nucl. Sci. 35, 1438-1443 (1988).

3. K. Lee, M. S. Shur, T. J. Drummond, and H. Morkoc, "Current-Voltage and Capacitance-Voltage Characteristics of Modulation-Doped Field-Effect Transistors," IEEE Trans. Electron Devices 30, 207-212 (1983).

4. F. F. Fang and W. E. Howard, "Negative Field-Effect Mobility on (100) Si Surfaces," Phys. Rev. Lett. 16, 797-799.

5. D. Delagebeaudeuf and N. T. Linh, "Metal-(n) AlGaAs-GaAs Two-Dimensional Electron Gas FET," IEEE Trans. Electron Devices 29, 955-960 (1982).

6. J. R. Brews, "A Charge Sheet Model of the MOSFET," Solid State Electron. 21, 345-355 (1978).

LABORATORY OPERATIONS

The Aerospace Corporation functions as an "architect-engineer" for national security projects, specializing in advanced military space systems. Providing research support, the corporation's Laboratory Operations conducts experimental and theoretical investigations that focus on the application of scientific and technical advances to such systems. Vital to the success of these investigations is the technical staff's wide-ranging expertise and its ability to stay current with new developments. This expertise is enhanced by a research program aimed at dealing with the many problems associated with rapidly evolving space systems. Contributing their capabilities to the research effort are these individual laboratories:

Aerophysics Laboratory: Launch vehicle and reentry fluid mechanics, heat transfer and flight dynamics; chemical and electric propulsion, propellant chemistry, chemical dynamics, environmental chemistry, trace detection; spacecraft structural mechanics, contamination, thermal and structural control; high temperature thermomechanics, gas kinetics and radiation; cw and pulsed chemical and excimer laser development, including chemical kinetics, spectroscopy, optical resonators, beam control, atmospheric propagation, laser effects and countermeasures.

Chemistry and Physics Laboratory: Atmospheric chemical reactions, atmospheric optics, light scattering, state-specific chemical reactions and radiative signatures of missile plumes, sensor out-of-field-of-view rejection, applied laser spectroscopy, laser chemistry, laser optoelectronics, solar cell physics, battery electrochemistry, space vacuum and radiation effects on materials, lubrication and surface phenomena, thermionic emission, photosensitive materials and detectors, atomic frequency standards, and environmental chemistry.

Electronics Research Laboratory: Microelectronics, solid-state device physics, compound semiconductors, radiation hardening; electro-optics, quantum electronics, solid-state lasers, optical propagation and communications; microwave semiconductor devices, microwave/millimeter wave measurements, diagnostics and radiometry, microwave/millimeter wave thermionic devices; atomic time and frequency standards; antennas, rf systems, electromagnetic propagation phenomena, space communication systems.

Materials Sciences Laboratory: Development of new materials: metals, alloys, ceramics, polymers and their composites, and new forms of carbon; nondestructive evaluation, component failure analysis and reliability; fracture mechanics and stress corrosion; analysis and evaluation of materials at cryogenic and elevated temperatures as well as in space and enemy-induced environments.

Space Sciences Laboratory: Magnetospheric, auroral and cosmic ray physics, wave-particle interactions, magnetospheric plasma waves; atmospheric and ionospheric physics, density and composition of the upper atmosphere, remote sensing using atmospheric radiation; solar physics, infrared astronomy, infrared signature analysis; effects of solar activity, magnetic storms and nuclear explosions on the earth's atmosphere, ionosphere and magnetosphere; effects of electromagnetic and particulate radiations on space systems; space instrumentation.